Cellulose (2023) 30:10825–10839
https://doi.org/10.1007/s10570-023-05563-4

ORIGINAL RESEARCH

Preparation, characterization and antibacterial properties of 4-aminocinnamic acid-modified cellulose fibers

Qinghui Duan · Pengxiang Shi · Jiaqi Huo · Mingjie Wang · Xingyu Lv · Dongmei Yang · Shujun Li · Xueren Qian

Received: 20 March 2023 / Accepted: 12 October 2023 / Published online: 29 October 2023

Abstract Cellulose materials do not possess any inherent antibacterial properties, which greatly limits their application in medical and food packaging fields. Antibacterial cellulose-based materials offer exciting properties and functionalities. However, they are normally prepared by using unstable physically absorbed or complicated chemically grafted antibacterial agents under harsh conditions. Herein, an eco-friendly and simple strategy is performed to fabricate long-term antibacterial cellulose-based materials. Initially, cellulose fibers (CFs) were modified by sodium periodate ($NaIO_4$) generating dialdehyde cellulose fibers (DCFs). Afterward, the 4-aminocinnamic acid was chemically grafted onto the DCFs yielding antibacterial CFs through Schiff base reaction. The 4-aminocinnamic modified DCFs (C-DCFs) exhibited excellent antibacterial activity against *S. aureus* and *E. coli*, with inhibition ratios greater than 99.6% and 99.0%, respectively. Quite encouragingly, the C-DCFs presented long-term antibacterial effectiveness, maintaining 99% antibacterial ratio after two months of exposure to the air environment. Therefore, grafting 4-aminocinnamic acid onto the CFs endowed the CFs with robust and sustained antibacterial properties that would make the material advantageous for use in relevant applications. Our strategy is efficient, green, easy to operate both in the work-up stage and purification, in conformity to principles of green chemistry.

Qinghui Duan and Pengxiang Shi contributed equally to this work.

Q. Duan · P. Shi · J. Huo · M. Wang · X. Lv · D. Yang (✉) · S. Li · X. Qian
Research Division for Sustainable Papermaking and Advanced Materials, Key Laboratory of Biobased Materials Science and Technology (Ministry of Education), Northeast Forestry University, Harbin, China
e-mail: yyddmm1980122@163.com

D. Yang
Hubei Provincial Key Laboratory of Green Materials for Light Industry, Hubei University of Technology, Wuhan, China

Graphical abstract

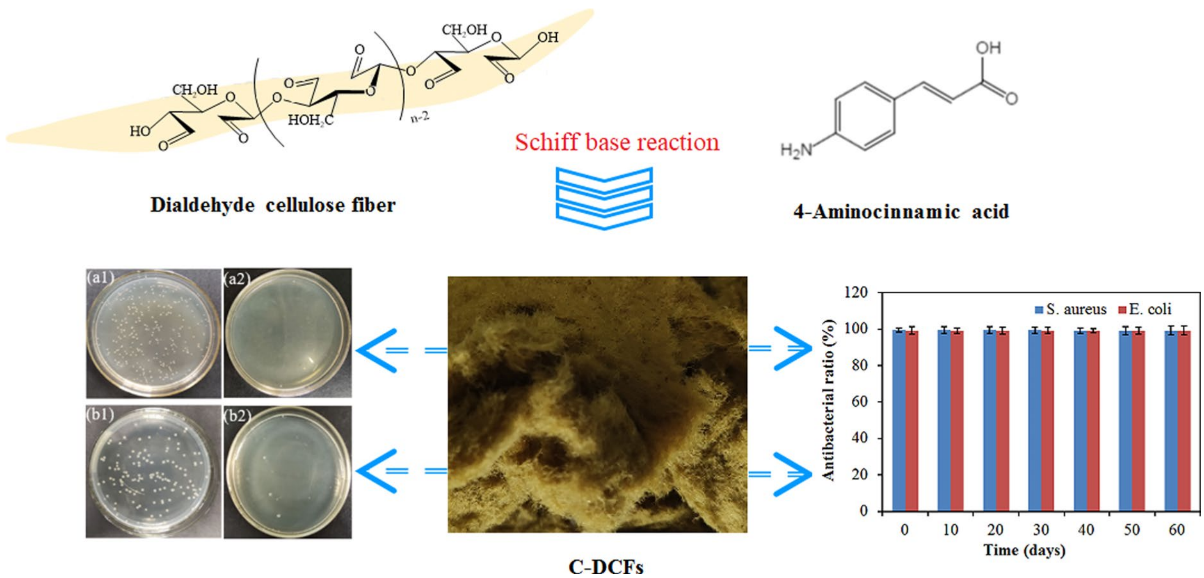

Keywords Dialdehyde cellulose fibers · Schiff base · 4-aminocinnamic acid · Antibacterial activity · Durability · Green chemistry

Introduction

Cellulose is the most abundant polysaccharide in nature and features a linear structure consisting of glucose monomers linked together through *β*-1,4-glycosidic bonds. As a renewable biopolymer, cellulose is nontoxic, biodegradable, and biocompatible (Rostami et al. 2019). However, cellulose itself does not have any antibacterial properties (Tavakolian et al. 2020) and is susceptible to microbial colonization and growth because of its porous structure and hygroscopicity (Cao et al. 2020), which severely limits its applications as a material, particularly in healthcare and food packaging (Cao et al. 2020).

Among the cellulose derivatives, dialdehyde cellulose (DAC) with unique structure and properties is an interesting material due to its wide application potential. Generally, DAC can be obtained through the oxidation of cellulose with $NaIO_4$. In order to overcome the problem of low oxidation efficiency caused by high-crystallinity and tight structure of cellulose, Zhang et al. (2023) developed a new preparation method of DAC with low energy consumption and chemical consumption, that is, cellulose raw materials were pretreated with $LiBr{\cdot}3H_2O$ to improve the accessibility of cellulose. As a result, the aldehyde group content of DAC was increased by around 30% and the production cost was reduced by 45%. Xu et al. (2023) comparatively studied the preparation methods of DAC using $NaIO_4$ pre-oxidation and synchronous oxidation via choline chloride (ChCl)/urea-based deep eutectic solvent (DES), the results showed that the two methods could obtain different micro-morphology, yield and aldehyde group content, which was an effective preparation strategy of DAC. As a polymeric dialdehyde similar to glutaraldehyde, the DAC was able to combine with proteins and nucleic acids of microbes by crosslinking, which may contribute to its antimicrobial activity (Zhang et al. 2017). The research report showed that the antibacterial activity of DAC against Gram-positive bacteria methicillin-resistant *S. aureus* (MRSA) (Luo et al. 2021; Mou et al. 2017) and Gram-negative bacteria *E. coli* (Mayer et al. 2021) increased in vitro with the increase of aldehyde group content, and it had biological safety and good biocompatibility. Unfortunately, DAC had poor antibacterial stability. The antibacterial activity of DAC gradually decreased with the extension of time, and basically disappeared after

7 days (He et al. 2021). Since microbial contamination and the emergence of new bacterial diseases can both significantly impact human health and safety, there is an urgent demand for new materials with robust and long-term antibacterial properties.

Considering that cellulose is a versatile and ubiquitous polymer, the ability to endow it with antibacterial properties would have tremendous implications in many fields that utilize cellulose-based materials (Sun et al. 2020). Endowing cellulose with antibacterial properties requires the loading of antibacterial agents onto cellulose fibers (CFs) through physical adsorption (Zhang et al. 2022; Zmejkoski et al. 2022; Hu et al. 2022) and/or chemical grafting (Dong et al. 2022; Catel-Ferreira et al. 2015; Fan et al. 2022). However, the physical adsorption of antibacterial agents is much weaker than chemical grafting and typically leads to the uncontrolled release of the adsorbed bacteriostatic agents, which will reduce the bacteriostatic performance of the cellulose-based materials over time and increase the risk of contaminating objects in contact with the cellulose-based materials (Fabrega et al. 2011; Poças et al. 2010). Therefore, the chemical bonding of antibacterial agents onto CFs is much more advantageous (Liu et al. 2010), as the antibacterial agents will not be as easily released from the CFs as those that are adsorbed through non-covalent interactions, meaning the material will maintain the antibacterial properties for longer periods of time (Saini et al. 2016a, b). The maintenance of antibacterial properties is highly advantageous, especially for objects with which people often have close contact, such as banknotes, stamps and clothes. In addition, there is significant utility for materials with robust antibacterial properties in food packaging, medical, and sanitary products.

Contact-active antibacterial surfaces have been developed using various molecular strategies, including the use of antibacterial peptides (Weishaupt et al. 2020), cationic polymers (Park et al. 2006; Tiller et al. 2001), quaternary ammonium compounds (Isquith et al. 1972), silanes (Saini et al. 2017; Hassanpour et al. 2018; Saini et al. 2016a, b), metal salts (Ibrahim et al. 2006), and *N*-halamines (Demir et al. 2015; Wang et al. 2022; Gouda et al. 2008). Schiff base-formation reactions, which are condensation reactions between an aldehyde (or ketone) and an amine to form an imine (Jia et al. 2015), are the most common reactions to chemically graft bacteriostatic agents onto cellulose because of the mild reaction conditions. The preparation of Schiff base materials is based on the integration of two efficient reactions: selective oxidation of cellulose using sodium periodate yielding dialdehyde cellulose and subsequent Schiff base reaction with compounds containing primary amines. Several cellulose-based Schiff base materials prepared by grafting nisin (Wu et al. 2019), L-lysine (Zhang et al. 2020), chitosan (Hou et al. 2008; Han et al. 2009), ε-polylysine (He et al. 2021), and glycine (Xu et al 2020) with dialdehyde cellulose have demonstrated suitable antibacterial properties.

Cinnamic acid, a naturally occurring phenylpropanoid derivative isolated from a variety of different plants and microorganisms, has low toxicity and can be metabolized in organisms (Sova 2012). Its antibacterial, antioxidant, and anticancer properties (Natella et al. 1999) make the compound advantageous for a wide variety of uses in flavors, fragrances, food additives, and medicine (Lafay and Gil-Izquierdo 2007). The bacteriostatic mechanism of cinnamic acid involves the destruction of the bacterial membrane, causing the cells to die (Cai et al. 2019). Cinnamic acid has demonstrated antibacterial activity against *E. coli*, *Salmonella enterica* (Whitney et al. 2008), and *Alicyclobacillus acidoterrestris* (Cai et al. 2015). In addition, cinnamic acid derived from *Capsicum annum* extracts were found to inhibit *Listeria monocytogenes*, *Bacillus cereus*, *S. aureus*, and *Salmonella typhimurium* (Dorantes et al. 2000), with a minimum inhibitory concentration (MIC) against *S. aureus* of 125 μg/mL (Mascotti et al. 2010).

Over time, the antibacterial properties of cinnamic acid physically adsorbed on CFs tend to gradually weaken. Therefore, it is more advantageous to chemically bind cinnamic acid to CFs, which has not been previously reported. In this work, to prevent leaching, cinnamic acid was chemically grafted onto CFs by first oxidizing the CFs into dialdehyde cellulose fibers (DCFs) by sodium periodate, after which the DCFs was modified with 4-aminocinnamic acid by reacting the amine with the aldehyde groups on the DCFs to generate Schiff bases (Scheme 1). The resulting C-DCFs were then characterized by SEM, FTIR, ^{13}C-NMR, XPS, XRD, and TGA. Following structural characterization, the antibacterial activities of the C-DCFs were inspected by the colony counting method. The preparation procedure of C-DCFs

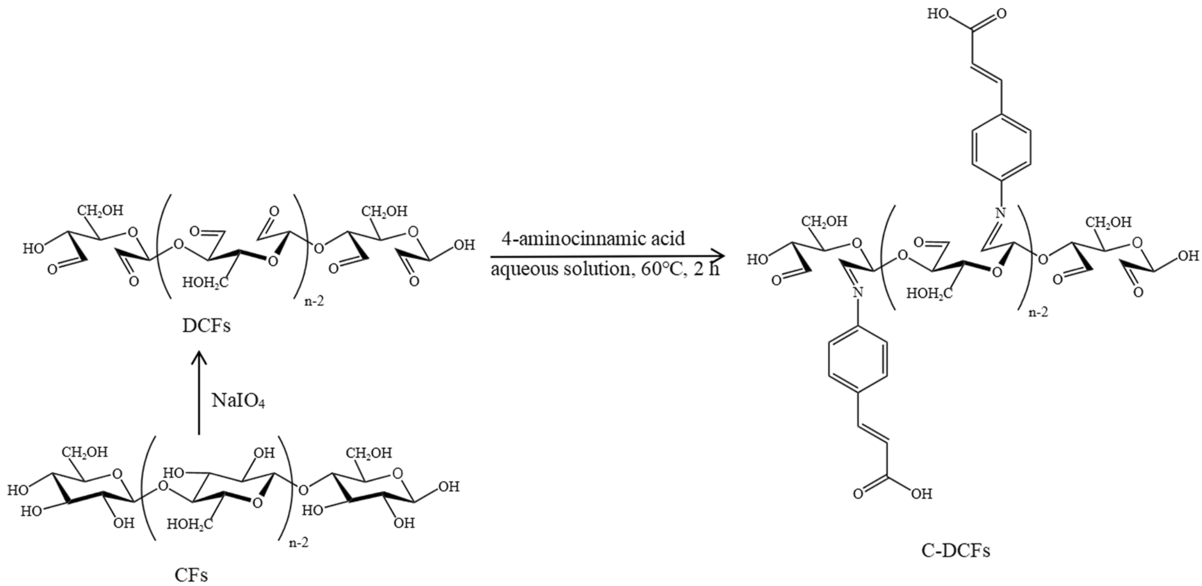

Scheme 1 Schematic diagram of 4-aminocinnamic acid grafted onto the DCFs

was performed in CFs suspension without any other solvent except water as the aqueous medium. Our approach may also offer promising opportunities for the preparation of other cellulose-based antibacterial materials, such as fabrics and textiles.

Materials and methods

Materials

Bleached kraft wood pulp was obtained from Mudanjiang Hengfeng Paper Co., Ltd. (Heilongjiang, China). 4-aminocinnamic acid was obtained from Biosynth Carbosynth Co., Ltd. (United Kingdom). Sodium periodate ($NaIO_4$) was purchased from Tianjin Yongda Chemical Reagent Co., Ltd. The bacterial culture medium was from Beijing Aoboxing Biotechnology Co., Ltd. *S. aureus* (ATCC25923-3) and *E. coli* (ATCC25922-3) were purchased from Qingdao Hi-Tech Park Haibo Biotechnology Co., Ltd. (Shandong, China).

Preparation of the DCFs

To prepare the DCFs, the wet bleached kraft wood pulp (20 g dry weight) was added to 750 mL of a 0.12 M $NaIO_4$ solution in deionized water. The pH of the suspension was adjusted to 4.0 with 1.0 mol/L HCl, and the system was stirred at 500 rpm and 50 °C for 4 h (Hou et al. 2008). After the oxidation was completed, the reaction was terminated by adding excess ethylene glycol. The DCFs were filtered by suction filtration, washed with deionized water, and a portion of the sample was dried for analysis and testing.

The aldehyde group's content of the DCFs was evaluated in accordance with the method reported by Zhang et al (2020). In this method, the aldehyde groups in the DCFs reacted with hydroxylamine hydrochloride, releasing hydrochloric acid that was neutralized with NaOH. Therefore, the volume of NaOH consumed was directly related to the aldehyde group content. The content of aldehyde groups in the DCFs was calculated to be 3.00 ± 0.03 mmol/g.

Preparation of the C-DCFs

Different amounts of 4-aminocinnamic acid were added to 70 mL of deionized water to prepare a series of solutions with different concentrations. The wet DCFs (1.0 g dry weight) were dispersed in 4-aminocinnamic acid solution, and the suspensions were continuously stirred for 2 h at 60 °C. Following, the modified DCFs (C-DCFs) were filtered by suction filtration, repeatedly washed with water to remove the free 4-aminocinnamic acid that was not adsorbed and dried in an oven at 60 °C for 6 h. The C-DCFs prepared with varying molar ratios of aldehydes to 4-aminocinnamic acid of 1:0.7, 1:1.0, and 1:1.3 were referred to herein as C-DCF1, C-DCF2, and C-DCF3, and their yields were 91.58%, 90.22%, and 88.03%, respectively.

SEM characterization

The DCFs and C-DCFs were sprayed with gold before observation under a JSM-7500F scanning electron microscope (JEOL). The micrographs of the DCFs and C-DCFs were observed at magnifications of 200 × and 1000 ×, respectively.

FT-IR characterization

A Vector22 infrared spectrometer (Bruker) was used to acquire FTIR spectra of the CFs, DCFs, and C-DCFs over the spectral window of 5000–500 cm^{-1} (resolution: 1 cm^{-1}, 16 scans). Potassium bromide (KBr) was mixed with ~ 20 mg of each of the dried samples, and the solid mixtures were pressed into tablets before analysis.

^{13}C-NMR characterization

Solid-state ^{13}C-NMR spectra of the C-DCFs were recorded on a Bruker 400 M spectrometer (Switzerland). The samples were spun at 10 kHz, the pre-scan delay was 6.5 μs, the rotor diameter was 4 mm, and the pulse program used for the acquisition was cp. The ^{13}C-NMR spectrum (liquid-phase) of 4-aminocinnamic acid was recorded on a Bruker 500 M spectrometer in deuterated water.

XPS characterization

XPS spectra of the CFs, DCFs, and C-DCFs were acquired on a X-ray photoelectron spectrometer (ESCALAB 250Xi, Thermo Fisher Scientific). Each sample was scanned at 1.0 eV per step and at an analyzer transfer energy of 160 eV.

Calculation of the substitution degree of 4-aminocinnamic acid

The degree of substitution (DS) of 4-aminocinnamic acid was calculated on the basis of the elemental composition of N, as determined by XPS (Sun et al. 2020). Since there are two O atoms, nine C atoms, seven H atoms, and one N atom per molecule of 4-aminocinnamic acid, the C content is nine times that of N, so the formula used to calculate the C content is shown in Eq. (1) below:

$$\%C_{4-\text{aminocinnamic acid}} = \%N \times 9 \tag{1}$$

Therefore, when the percentage of C atoms in 4-aminocinnamic acid is known, the % C in the anhydroglucose unit (AGU) was calculated using Eq. (2) below:

$$\%C_{AGU} = \%C_{total} - \%C_{4-\text{aminocinnamic acid}} \tag{2}$$

In one AGU, which contains six carbon atoms, there are two O atoms that can participate per oxidation reaction. Thus, the percentage of reactive O atoms per AGU was calculated using Eq. (3) below:

$$\%O_{AGU} = \%C_{AGU} \times 2/6 \tag{3}$$

Finally, the DS of 4-aminocinnamic acid was calculated using Eq. (4) below:

$$DS = \%N/\left(\%O_{AGU}\right) \tag{4}$$

XRD characterization

XRD spectra of the CFs, DCFs, and C-DCFs were acquired on a D/max2200VPC diffractometer (Rigaku, Japan). The samples were scanned over the range of 0–70° at a scan rate of 5°/min, a scanning step of 0.02° (current: 30 mA, voltage: 40 kV). The data were subtracted from a blank run (air) to remove the environmental background. The crystallinity index (CrI, %) (French 2014) was calculated using Eq. (5) below:

$$CrI(\%) = \frac{I_{200} - I_{am}}{I_{200}} \times 100 \tag{5}$$

wherein I_{200} is the intensity of diffraction peak of (200) lattice plane, and I_{am} is the intensity of the minimum between the 110 and 200 peaks at about 18.5° attributed to amorphous cellulose.

TGA characterization

The CFs, DCFs, and C-DCF samples were measured using a TGA 5500 (TA Instruments, United States). Each sample (10 mg) was placed on a platinum crucible and heated from 50 to 600 °C at a heating rate of 10 °C/min under a pure nitrogen atmosphere with a flow rate of 50 mL/min.

Antibacterial assessment

The colony counting method was performed to quantitate the antibacterial activities of the C-DCFs (Sun et al. 2020). Each experiment was performed in triplicate. A two-step pre-cultivation process was used to prepare the bacterial inoculum suspension. All test bacteria were activated, diluted with a nutrient broth, and transferred to 0.03 mol/L PBS buffer, and the medium was mixed thoroughly and diluted to 10^5–10^6 CFU/mL with viable bacteria to inoculate each cellulose sample. Next, the diluted suspensions were sterilized at 121 °C and 103 kPa for 30 min in an autoclave. The samples (0.1 g) were dispersed into a mixture of the inoculum (1 mL) and 0.03 mol/L PBS buffer (25 mL) in a 50 mL triangular flask. The untreated cellulose was used as a blank control. The flasks were covered with bottle stoppers and incubated in a constant temperature shaker at 37 °C while shaking at 140 r/min for 24 h. Then, 1 mL of each test solution was removed from its respective flask, transferred to a test tube containing 9 mL of 0.03 mol/L PBS buffer, and mixed thoroughly. The solutions were serially diluted tenfold, after which 100 μL of the bacterial suspension at each dilution factor was removed from the test tubes to inoculate nutrient agar plates, which were incubated upside down at 37 °C for 18 h. A plate with a dilution factor between 30 and 300 CFU was chosen for counting. In addition, long-term antibacterial activity experiments were conducted, in which the C-DCFs were placed in an air environment. The antimicrobial ratios of the C-DCFs were tested for every 10 days.

The antibacterial ratio was calculated using Eq. (6) below:

$$\text{Antibacterial ratio } (\%) = \text{X} - \text{Y}/\text{X} \times 100\% \tag{6}$$

wherein X and Y are the average numbers of viable bacteria in the flasks containing the blank sample and Schiff base sample, respectively, after incubating for 18 h.

The bacteria log reduction of the samples was calculated using Eq. (7) below:

$$\begin{aligned} \text{log reduction} = {} & \text{log CFU } \text{T}_{18}\text{blank (control)} \\ & - \text{log CFU } \text{T}_{18}\text{(sample)} \end{aligned} \tag{7}$$

In the standard dynamic shake flask method, at least a 1 log reduction in bacteria load is required to claim antibacterial properties (Saini et al. 2016a, b).

Results

Surface topography

Images of the macroscopic and microscopic morphologies of DCFs and C-DCF2 acquired by a digital camera and SEM are shown in Fig. 1. After the loading of 4-aminocinnamic acid onto the DCFs, the color of the DCFs underwent a significant change from milk white to dark, and the dark green color of C-DCF2 did not fade after repeated washing, indicating that the bacteriostatic agent had been chemically grafted onto the DCFs substrate (Fig. 1a, d). As determined by SEM, the morphology of DCFs was obviously bent and twisted, and the fibers were relatively complete and had no obvious fractures, while the morphology of C-DCF2 was relatively straight and had obvious fractures, which might have been attributed to the introduction of 4-aminocinnamic acid that changed the fiber morphology of the DCFs (Xu et al. 2020) (Fig. 1b, e). These differences in morphology were more pronounced when observed at higher magnifications (Fig. 1c, d).

Analysis of the FTIR

The FTIR spectra of CFs, DCFs, and the C-DCFs are shown in Fig. 2. The spectrum of the CFs featured two absorption bands at 3415 cm^{-1} (–OH stretching) and 2907 cm^{-1} (symmetric C–H vibrations) (Keshk and Haija 2011). In addition, the

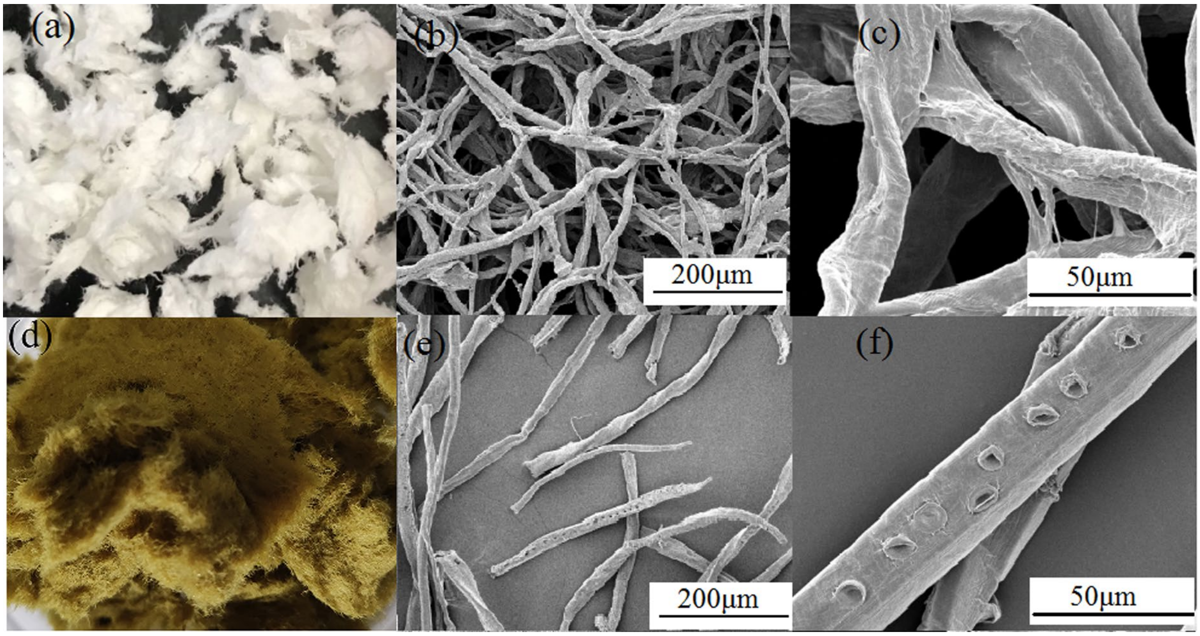

Fig. 1 Surface topography of the samples. **a** and **d** Photographs of DCFs and C-DCF2, respectively, **b** and **c** SEM images of DCFs, and **e** and **f** SEM images of C-DCF2

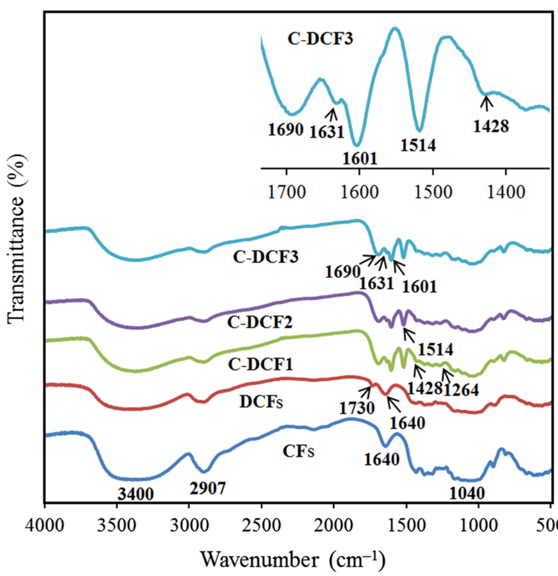

Fig. 2 FTIR spectra of the CFs, DCFs, and C-DCFs

absorption band at 1040 cm^{-1} was ascribed to C – O stretching vibrations (Liu et al. 2011), and the absorption band at 1640 cm^{-1} was due to the absorbed water (Sun et al. 2015a, b). In the spectrum of the DCFs, a characteristic band at 1733 cm^{-1} was observed, which was assigned to C=O stretching vibrations (He et al. 2021), indicating that the aldehyde group had been formed. In the C-DCFs, the characteristic band at 1733 cm^{-1} disappeared, while new band at 1631 cm^{-1} appeared, which were derived from the C=N bonds of the imine group formed by the condensation between the aldehydes in the DCFs and 4-aminocinnamic acid (Song et al. 2022; Gadkari et al. 2019). The absorbance band at 1690 cm^{-1} corresponded to the C=O stretching vibrations of the carboxylic acid group in the 4-aminocinnamic acid, while the absorption bands at 1601 cm^{-1}, 1514 cm^{-1}, and 1428 cm^{-1} were ascribed to the skeletal vibrations of the benzene ring of cinnamic acid; furthermore, the absorption band at 1264 cm^{-1} corresponded to C – N bending vibrations (Keshk et al. 2015). Lastly, in the FTIR spectrum of the C-DCFs, the missing characteristic band at 1733 cm^{-1} and the appearance of the new absorption band at 1631 cm^{-1} confirmed that the imine bond had formed between the C=O group in the DCFs and the -NH_2 group of 4-aminocinnamic acid.

Analysis of the ^{13}C NMR spectra

The liquid-phase ^{13}C NMR spectrum of 4-aminocinnamic acid and the solid-state ^{13}C NMR spectra of the DCF2 and the C-DCF2 are shown in Fig. 3. As shown in Fig. 3a, the C1 resonance of the carboxylic acid group appeared at 169.8 ppm, and the signals at 144.1 and 118.4 ppm were assigned to C2 and C7 of unsaturated double bond, respectively. The resonances at 134.3, 131.4, 129.6, and 123.3 ppm were assigned to C3, C4, C5, and C6 of benzene ring, respectively.

After oxidation by periodate (Fig. 3b), the signals of the DCF2 detected at 105.2, 89.0, 74.9, 72.4, 71.9 and 65.3 ppm were assigned to C1’, C4’, C2’, C3’, C5’ and C6’ of anhydroglucose units (AGU), and the appearing signal at 95.7 ppm originated from hemiacetal structures between two aldehyde groups (Siller et al. 2015). In the solid-state ^{13}C NMR spectrum of C-DCF2 (Fig. 3c), the signals were observed at 170.6, 161.6, 146.9, 128.5, 115.9, 105.0, 89.0, 74.1, 72.1, and 65.7 ppm. The signals at 170.6, 146.9, and 115.9 ppm were ascribed to the C1, C2, and C7 of 4-aminocinnamic acid, respectively, while the signals at 128.5 ppm represented the cluster of resonances of the C3, C4, C5, and C6 of 4-aminocinnamic acid. The signal at 105.0 ppm was ascribed to C1’ of the AGU, the signal at 65.7 ppm represented the C6’ (Davies et al. 2002) of the AGU, the signal peak at 89.0 ppm was associated to C4’ of the AGU, and the cluster of

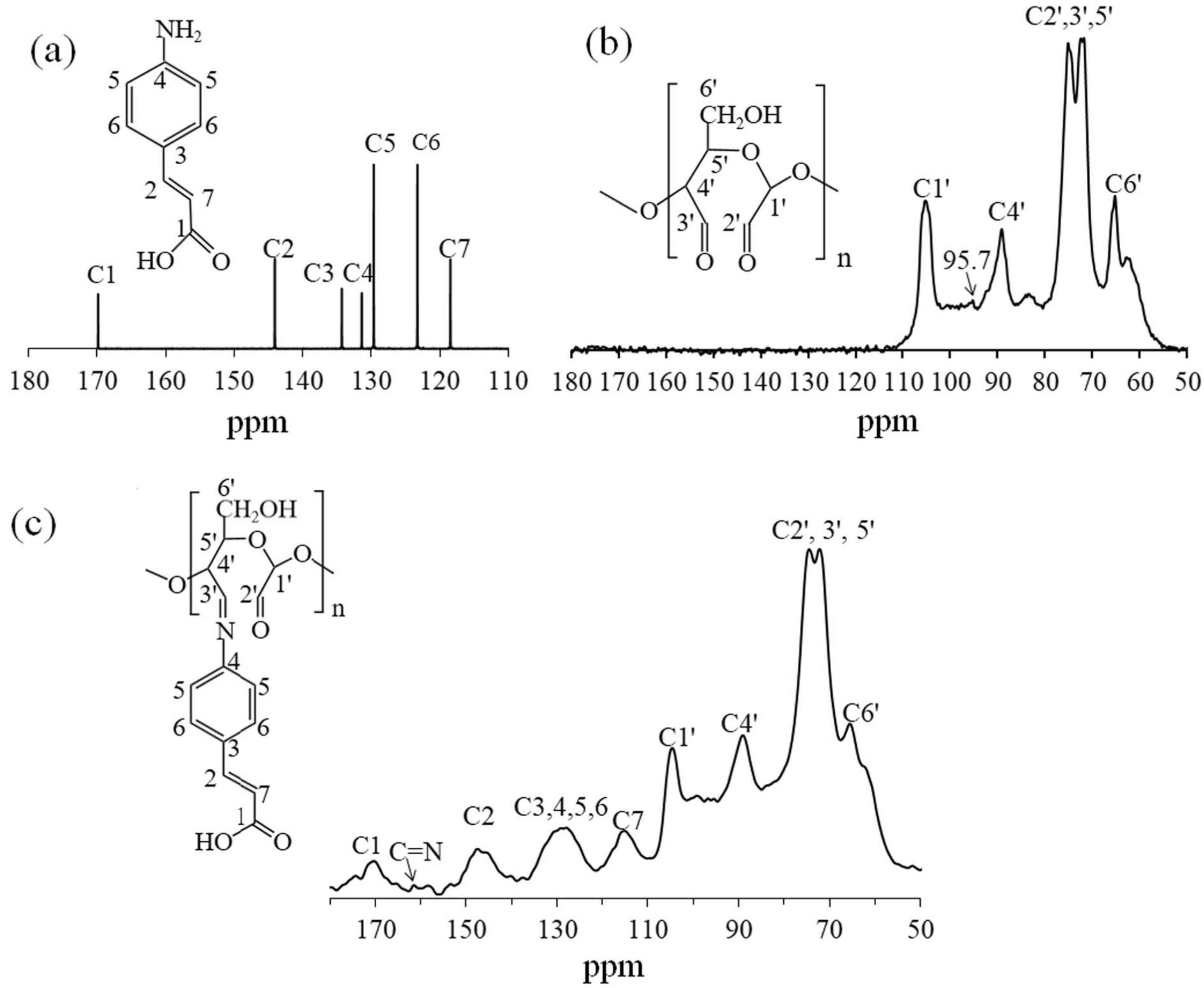

Fig. 3 **a** Liquid-phase ^{13}C-NMR spectrum of 4-aminocinnamic acid, **b** and **c** solid-state ^{13}C-NMR spectra of DCF2 and C-DCF2, respectively

resonances between 70 and 81 ppm were ascribed to the C2’, C3’, and C5’ atoms of the AGU (Maunu et al. 2000). The signal representing the hemiacetal structure disappeared. Lastly, the signal at 161.6 ppm in the C-DCF2 spectrum was assigned to the C=N group (Zhang et al. 2020).

Analysis of the XPS

The XPS spectra of the CFs, DCFs, and C-DCFs are shown in Fig. 4, and the elemental atomic percentages of the materials are provided in Table 1. As shown in Fig. 4a, the XPS spectra of the CFs and DCFs featured characteristic peaks at 531.1 eV and 284.8 eV, indicating that both materials comprised only O and C elements, respectively. In the C-DCFs, a new signal peak appeared at 399.1 eV that corresponded to an N1s peak (Sun et al. 2020). The high-resolution C1s spectrum of the DCFs (Fig. 4b), as well as the high-resolution C1s (Fig. 4c) and N1s (Fig. 4d) spectra of the C-DCFs, provided information on chemical states of the atoms in the materials. The chemical shifts of the carbon (C1s) atoms in the DCFs could be divided into four categories (Gao et al. 2012): O–C=O, C=O (or O–C–O), C–O, and C–C, with peaks centered at 288.6, 287.8, 286.6, and 284.8 eV, respectively. In the high-resolution C1s spectrum of the C-DCFs, two additional peaks appeared at 287.3 and 286.7 eV, which were ascribed to C=N and C–N groups, respectively (Lin et al. 2008). The high-resolution N1s spectrum of the surface of the C-DCFs featured a peak at 398.9 eV, which was attributed to the = N– atom of the Schiff base (Lebrini et al. 2007; Bentiss et al. 1999). The peak corresponding to the N–H group was not observed in the high-resolution N1s spectra, which indicated that there were no free 4-aminocinnamic acid molecules in the modified fibers. As shown in Table 1, as the proportion of 4-aminocinnamic acid in the C-DCFs increased from 0.7:1 to 1.3:1, the atomic percentage of N increased from 4.23 to 6.10%. By calculation, the substitution degree of 4-aminocinnamic acid on the surface of the C-DCFs ranged from 0.33 to 1.12. These results indicated that 4-aminocinnamic acid was successfully grafted onto the DCFs.

Table 1 Elemental composition of the CFs, DCFs, and C-DCFs determined by XPS

Samples	C1s (%)	O1s (%)	N1s (%)	DS
CFs	72.56	27.44	–	–
DCFs	67.26	32.74	–	–
C-DCF1	76.73	19.04	4.23	0.33
C-DCF2	74.55	20.02	5.43	0.63
C-DCF3	71.18	22.72	6.10	1.12

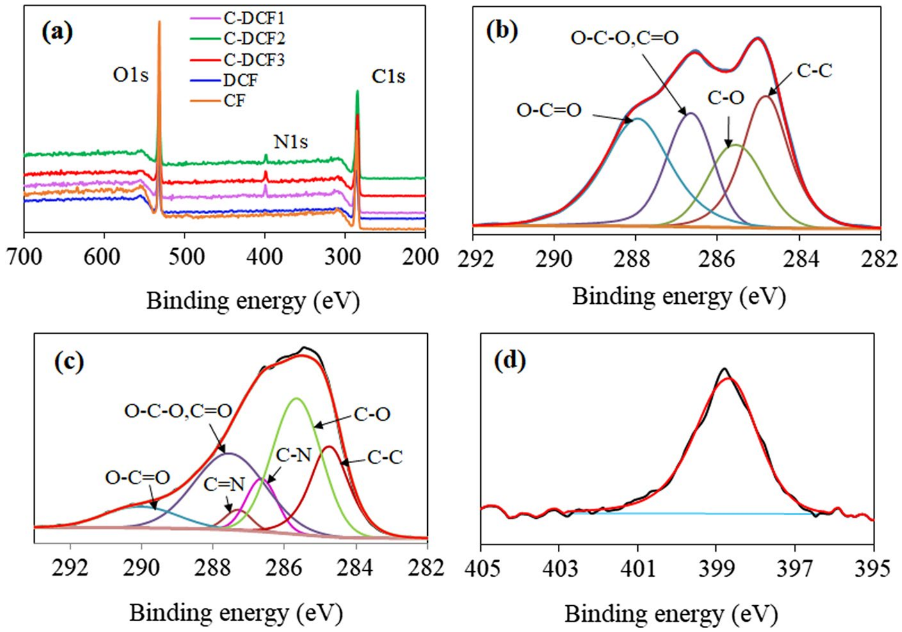

Fig. 4 **a** XPS spectra of the CFs, DCFs, and C-DCFs, **b** high-resolution C1s XPS spectra of the DCFs, **c** and **d** high-resolution C1s and N1s XPS spectra of the C-DCF2

Analysis of the XRD

The XRD patterns of the CFs, DCFs, and the C-DCFs are shown in Fig. 5. The XRD pattern of the CFs featured four diffraction peaks at $2\theta = 14.9°, 16.7°, 22.5°$, and 34.5° (French 2014). The maximum peak at 22.5° was due to the (200) lattice plane of lattice structure of the cellulose I, and the two overlapping peaks at 14.9° and 16.7° were ascribed to the (1–10) and (110) lattice planes, respectively (French 2014; Park et al. 2010; Sun et al. 2015a, b). The CrI value of the CFs was calculated to be 60.76%. However, after oxidation, the peaks at $2\theta = 14.9°, 16.7°$ and 22.5° became much broader, and the CrI value of the DCFs dropped significantly to 47.06%. This was attributed to the oxidation of cellulose by $NaIO_4$, which caused the glucose rings to open, thereby destroying the highly ordered structure of the cellulose molecules (Kim et al. 2000). Compared to the DCFs, the peaks at $2\theta = 14.9°$, 16.7°, and 22.5° in the XRD pattern of the C-DCFs became much broader, and the intensity become weaker. The CrI values of C-DCF1, C-DCF2, and C-DCF3 were 41.14%, 34.52%, and 31.04%, respectively. Compared to the DCFs, the C-DCFs had relatively low CrI values, indicating that the generation of the Schiff base linker between the DCFs and 4-aminocinnamic acid reduced the crystallinity of DCFs.

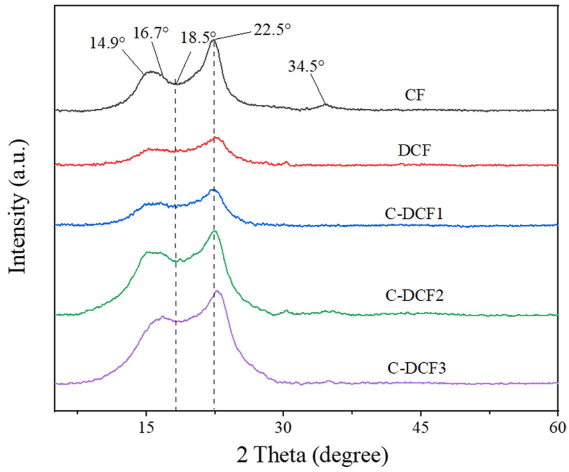

Fig. 5 XRD patterns of the CFs, DCFs, and C-DCFs

Thermogravimetric analysis (TGA)

To determine whether the grafting of 4-aminocinnamic acid onto the DCFs changed the thermal stability of the DCFs, the CFs, as well as the DCFs and C-DCFs, underwent TGA. As shown in Fig. 6, the initial mass loss of the CFs, the DCFs, and the C-DCF2 represented 5–10% of the total mass loss, which was ascribed to the loss of absorbed water (Siller et al. 2015). The CFs underwent a noticeable decomposition beginning at ~ 290 °C (Fig. 6a), and its corresponding DTG peak temperature was observed at around 340 °C (Fig. 6b), while the DCFs exhibited a more pronounced decomposition at lower temperature (245 °C) (Fig. 6a), and its corresponding DTG peak temperature was observed at around 300 °C (Fig. 6b). The difference in the temperature at which the CFs and DCFs underwent thermal decomposition might have been due to the highly orderly arrangement of the cellulose chains in the crystal structure of the CFs, which prevented the non-thermoplastic melting of cellulose (Visakh et al. 2010). However, after oxidation, the opening of the glucopyranose rings resulted in a reduction of the orderly packing of cellulose chains, thereby reducing the crystallinity

Fig. 6 TGA and DTG curves of the CFs, DCFs, and C-DCF2

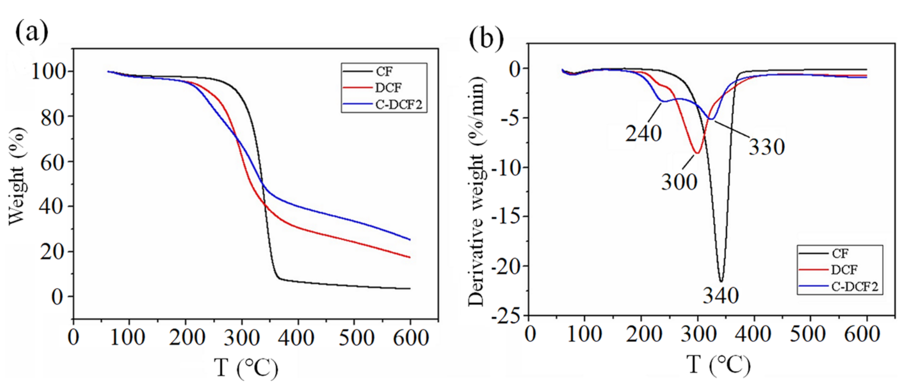

of the DCFs and causing the decomposition temperature of the DCFs to shift to lower temperature. For the C-DCF2, a more significant thermal decomposition occurred at 210 °C (Fig. 6a) was observed. And its DTG peaks were observed at 240 °C and 330 °C (Fig. 6b), this may be caused by the thermal decomposition of cinnamic acid (Zhao et al. 2014) and cellulose with aldehyde group and C=N bond. Therefore, TGA and DTG analysis showed that the introduction of 4-aminocinnamic acid increased the thermal stability of cellulose materials.

Antibacterial activity

The antibacterial ratios of the C-DCFs were also quantitatively measured using the colony counting method. As shown in Table 2, after the C-DCFs were exposed to bacterial suspensions of each organism for 18 h, the antibacterial ratios of the DCF2 against *E. coli* and *S. aureus* were 69.4% and 71.8%, respectively, and the antibacterial ratios of the C-DCFs against *E. coli* and *S. aureus* were greater than 99.0% and 99.6%, respectively. For the two bacteria, the log reduction numbers of the DCF2 were about 0.5, while the log reduction numbers of the C-DCFs were greater than 2.0. Compared with the DCF2, the C-DCFs exhibited better inhibitory effect against two tested bacteria, which is very important for the potential applications. The numbers of colonies grown in the culture dishes are shown in Fig. 7a, b. The numbers of bacterial colonies in the culture dishes containing the suspension treated with C-DCF2 at the same dilution level were significantly lower than in the dishes of the control group, indicating that the C-DCF2 materials more significantly inhibited the growth of the bacteria after contact with the bacterial suspension.

To evaluate the antibacterial durability of the C-DCFs, we exposed the samples to an air environment under ambient conditions for 2 months and measured the antibacterial activities of each C-DCFs sample at different time periods. As shown in Fig. 7c, the C-DCFs retained more than 99.0% of their antibacterial activity, even after two months, demonstrating their long-lasting antibacterial properties.

In Table 3, the antibacterial ratio was compared between the synthesized C-DCFs and other studies. As shown in Table 3, the antibacterial ratios of C-DCFs were markedly higher than the ratio of other chemically loaded materials; however, some materials prepared using physical impregnation methods were higher than the C-DCFs prepared in this study. The potent antibacterial properties of the C-DCFs might have been due to the combination of the imine groups and grafted cinnamic acid.

Conclusion

We propose a simple and green strategy to convert CFs into cellulose-based antibacterial materials by combining two efficient reactions: oxidation of CFs yielding DCFs as well as Schiff base reaction between DCFs and 4-aminocinnamic acid generating antibacterial CFs. This strategy is highly advantageous for large-scale industrial applications because the synthetic process is highly sustainable. It was verified by FTIR and XPS spectra that CFs was successfully grafted with 4-aminocinnamic acid. The C-DCFs materials demonstrated remarkable and stable antibacterial properties against *S.*

Table 2 Antibacterial ratios and parameters of C-DCFs against *S. aureus* and *E. coli*

Bacteria	Samples	Contact time (hours)		Antibacterial ratio (%)	Log reduction
		0	18		
S. aureus(CFU/mL)	DCF2	1.61×10^7	4.90×10^6	71.8 ± 1.02	0.52
	C-DCF1	2.29×10^7	1.0×10^5	99.6 ± 1.41	2.36
	C-DCF2	2.29×10^7	0	100 ± 0	–
	C-DCF3	2.29×10^7	0	100 ± 0	–
E. coli(CFU/mL)	DCF2	1.71×10^7	4.80×10^6	69.4 ± 0.72	0.55
	C-DCF1	1.32×10^7	1.33×10^5	99.0 ± 0.88	2.00
	C-DCF2	1.32×10^7	6.50×10^4	99.5 ± 1.33	2.31
	C-DCF3	1.32×10^7	0	100 ± 0	–

"–" means that it cannot be calculated

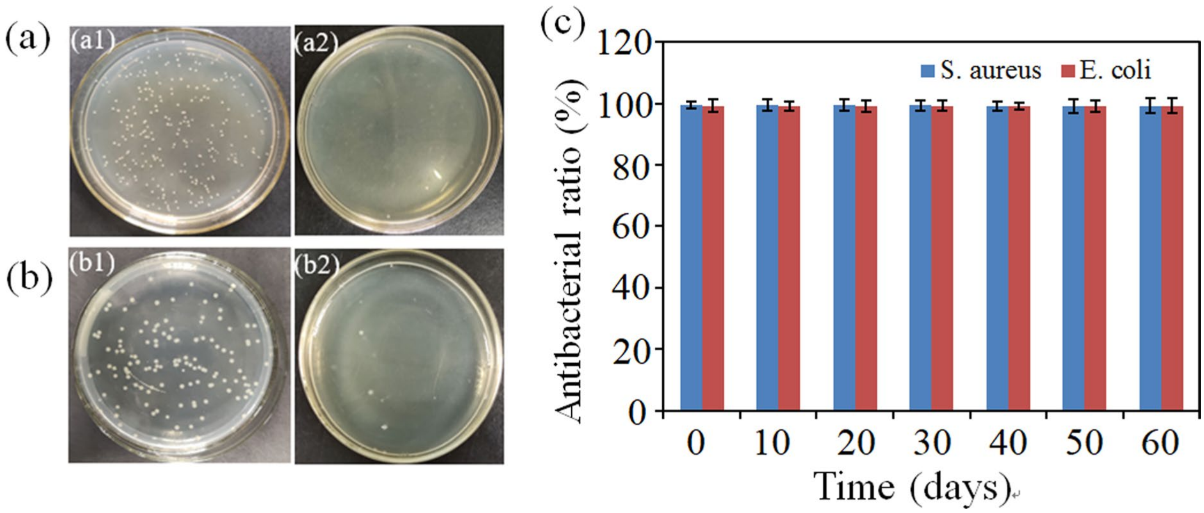

Fig. 7 Antibacterial effect of the C-DCFs. Photos of the *S. aureus* control (**a1**) and C-DCF2 (**a2**); photos of the *E. coli* control (**b1**) and C-DCF2 (**b2**); long-term antibacterial activity of C-DCF2 (**c**)

Table 3 Comparison of the antimicrobial effect between the modified cellulose materials and other known cellulose derivatives

Material	Antimicrobial effect (anti-bacterial ratio %) against microbial strain		References
	on *S. aureus*	on *E. coli*	
Bacterial cellulose with chitooligosaccharide	99.6	90.6	Yin et al. (2019)
CNC/Fe-Cu (coating)	95.9	98.8	Chen et al. (2020)
Viscose fibers with ε-polylysine	–	90.48	Gao et al. (2017)
Cellulose acetate sorbate	95.4	81.5	Wei et al. (2020)
Cellulose with octadecyldimethyl (3-trimethoxysilylpropyl)ammonium chloride	> 99	96–99	Andresen et al. (2007)
Cellulose fiber sheets/silver (impregnation)	91.58–99.46	93.6–99.78	Csóka et al. (2012)
Cellulose/quaternary ammonium salt (impregnation)	100.0	53.4–100.0	Wei et al. (2020)
cellulose triacetate with (3-chloro-2-hydroxypropyl)trimethylammonium chloride	64.7–76.6	78.7–89.0	Fei et al. (2018)
Cellulose nanocrystals with 2-(dimethylamino)ethyl methacrylate	75.48–98.72	72.25–98.64	Li et al. (2018)
Cellulose with quaternary ammonium salts	98	84	Jia et al. (2019)
Cellulose with 4-aminocinnamic acid	99.6–100	99.0–100	Present study

aureus and *E. coli*, with antibacterial ratios greater than 99.0%. Moreover, the C-DCFs presented long-term antibacterial effectiveness, maintaining 99% antibacterial ratio after two months of exposure to the air environment. The long-term antibacterial performance of C-DCFs is mainly due to the fact that the chemically grafted 4-aminocinnamic acid is non-leaching and kills bacteria by contact. We anticipate that these modified cellulose materials will have extensive applications in the fields of daily contact products, healthcare, and food packaging.

Acknowledgments This work was supported by the Fundamental Research Funds for the Central Universities (2572020BB06) and Open Research Foundation of Hubei

Provincial Key Laboratory of Green Materials for Light Industry (202307B01).

Author contributions QD: designed the study, performed the research, analyzed the data, and wrote the paper. PS: conceived the study and collected the data. JH: carried out the literature search and analyzed the data. MW: carried out the supplementary experiments. XL: conceived the study and analyzed the data. DY: conceived the study, designed the study, and provided the foundation support. SL: conceived the study and collected important background information. XQ: provided assistance in data acquisition. All authors reviewed the manuscript.

Funding This work was supported by the Fundamental Research Funds for the Central Universities (Grant No. 2572020BB06) and Open Research Foundation of Hubei Provincial Key Laboratory of Green Materials for Light Industry (202307B01).

Availability of data and materials Not applicable.

Declarations

Competing interests The authors declare no competing interests.

Conflict of interest All authors declare that they have no known competing financial interests or personal relationships that could have appeared to influence the work reported in this paper.

Ethics approval and consent to participate Not applicable.

Consent for publication Not applicable.

References

Andresen M, Stenstad P, Møretrø T, Langsrud S, Syverud K, Johansson LS, Stenius P (2007) Nonleaching antimicrobial films prepared from surface-modified microfibrillated cellulose. Biomacromol 8:2149–2155

Bentiss F, Traisnel M, Gengembre L, Lagrenée M (1999) A new triazole derivative as inhibitor of the acid corrosion of mild steel: electrochemical studies, weight loss determination, SEM and XPS. Appl Surf Sci 152:237–249

Cai R, Yuan Y, Wang Z, Guo C, Liu B, Pan C, Liu L, Yue T (2015) Effects of preservatives on Alicyclobacillus acidoterrestris growth and guaiacol production. Int J Food Microbiol 214:145–150

Cai R, Miao M, Yue T, Zhang Y, Cui L, Wang Z, Yuan Y (2019) Antibacterial activity and mechanism of cinnamic acid and chlorogenic acid against alicyclobacillus acidoterrestris vegetative cells in apple juice. Int J Food Sci 54:1697–1705

Cao Y, Gu J, Wang S, Zhang Z, Yu H, Li J, Chen S (2020) Guanidine-functionalized cotton fabrics for achieving permanent antibacterial activity without compromising their physicochemical properties and cytocompatibility. Cellulose 27(10):6027–6036

Catel-Ferreira M, Tnani H, Hellio C, Cosette P, Lebrun L (2015) Antiviral effects of polyphenols: development of bio-based cleaning wipes and filters. J Virol Methods 212:1–7

Chen L, Yu H, Deutschman C, Yang T, Tam KC (2020) Novel design of Fe-Cu alloy coated cellulose nanocrystals with strong antibacterial ability and efficient Pb^{2+} removal. Carbohydr Polym 234:115889

Csóka L, Božanic DK, Božanic DK, Nagy V, Dimitrijevic-Brankovic S, Luyt AS, Grozdits G, Djokovic V (2012) Viscoelastic properties and antimicrobial activity of cellulose fiber sheets impregnated with Ag nanoparticles. Carbohydr Polym 90:1139–1146

Davies LM, Harris PJ, Newman RH (2002) Molecular ordering of cellulose after extraction of polysaccharides from primary cell walls of Arabidopsis thaliana: a solid state CP/MAS 13C NMR study. Carbohydr Res 337:587–593

Demir B, Cerkez I, Worley SD, Broughton RM, Huang T-S (2015) N-halamine-modified antimicrobial polypropylene nonwoven fabrics for use against airborne bacteria. ACS Appl Mater Inter 7:1752–1757

Dong X, Wang H, Zhang H, Li M, Huang Z, Wang Q, Li X (2022) Copper-thiosemicarbazone complexes conjugated-cellulose fibers: biodegradable materials with antibacterial capacity. Carbohydr Polym 294:119839

Dorantes L, Colmenero R, Hernandez H, Mota L, Jaramillo ME, Fernandez E, Solano C (2000) Inhibition of growth of some foodborne pathogenic bacteria by Capsicum annum extracts. Int J Food Microbiol 57:125–128

Fabrega J, Luoma SN, Tyler CR, Galloway TS, Lead JR (2011) Silver nanoparticles: behaviour and effects in the aquatic environment. Environ Int 37:517–531

Fan B, Qi B, Wang P, Liu Y, Yu Y, Wang Q, Ren X (2022) Mechanically tough and regenerable antibacterial nanofibrillated cellulose-based aerogels for oil/water separation. Langmuir 38(34):10716–10727

Fei P, Liao L, Meng J, Cheng B, Hu X, Song J (2018) Non-leaching antibacterial cellulose triacetate reverse osmosis membrane via covalent immobilization of quaternary ammonium cations. Carbohyd Polym 181:1102–1111

French A (2014) Idealized powder diffraction patterns for cellulose polymorphs. Cellulose 21(2):885–896

Gadkari RR, Suwalka S, Yogi MR, Ali W, Das A, Alagirusamy R (2019) Green synthesis of chitosan-cinnamaldehyde cross-linked nanoparticles: characterization and antibacterial activity. Carbohydr Polym 226:115298

Gao S, Gao R (2017) Antibacterial cellulose composite membranes prepared in ionic liquid via phase inversion method. Chem Res Chin Univ 33(4):678–683

Gao C, Yan T, Dai K, Wan Y (2012) Immobilization of gelatin onto natural nanofibers for tissue engineering scaffold applications without utilization of any crosslinking agent. Cellulose 19:761–768

Gouda M, Ibrahim NA (2008) New approach for improving antibacterial function to cotton fabric. J Ind Text 37(4):327–339

Han S, Lee M (2009) Crosslinking reactions of oxidized cellulose fiber. II. Reactions between dialdehyde cellulose and

chito-oligosaccharides on lyocell fabric. J Appl Polym Sci 112:709–714
Hassanpour A, Asghari S, Lakouraj M M, Mohseni M (2018) Preparation and characterization of contact active antibacterial surface based on chemically modified nanofibrillated cellulose by phenanthridinium silane salt. Int J Biol Macromol 115:528–539
He X, Li Y, Zhang L, Du R, Dai Y, Tan Z (2021) Preparation of 2,3-dialdehyde microcrystalline cellulose particles crosslinked with epsilon-poly-L-lysine and their antibacterial activity. Cellulose 28:2833–2847
Hu X, Liu Y, Zhu D, Jin Y, Jin H, Sheng L (2022) Preparation and characterization of edible carboxymethyl cellulose films containing natural antibacterial agents: Lysozyme. Food Chem 385:132708
Hou Q, Liu W, Liu Z, Duan B, Bai L (2008) Characteristics of antimicrobial fibers prepared with wood periodate oxycellulose. Carbohydr Polym 74:235–240
Ibrahim NA, Abo-Shosha MH, El-Shafei AM, Abdel Fatah OM, Gaffar MA (2006) Antibacterial properties of ester-crosslinked cellulose-containing fabrics post treated with metal salts. Polym Plastic Technol Eng 45(6):719–727
Isquith AJ, Abbott EA, Walters PA (1972) Surface-bonded antimicrobial activity of an organosilicon quaternary ammonium chloride. Appl Microbiol 24:859–863
Jia Y, Li J (2015) Molecular assembly of Schiff base interactions: construction and application. Chem Rev 115:1597–1621
Jia R, Tian W, Bai H, Zhang J, Wang S, Zhang J (2019) Sunlight-driven wearable and robust antibacterial coatings with water-soluble cellulose-based photosensitizers. Adv Healthc Mater 8(5):1801591
Keshk S, Haija MA (2011) A new method for producing microcrystalline cellulose from Gluconacetobacter xylinus and kenaf. Carbohydr Polym 84:1301–1305
Keshk SMAS, Ramadan AM, Bondock S (2015) Physicochemical characterization of novel Schiff bases derived from developed bacterial cellulose 2,3-dialdehyde. Carbohydr Polym 127:246–251
Kim UJ, Kuga S, Wada M, Okano T, Kondo T (2000) Periodate oxidation of crystalline cellulose. Biomacromol 1:488–492
Lafay S, Gil-Izquierdo A (2007) Bioavailability of phenolic acids. Phytother Res 7:301–311
Lebrini M, Lagrene M, Traisnel M, Gengembre L, Vezin H, Bentiss F (2007) Enhanced corrosion resistance of mild steel in normal sulfuric acid medium by 2,5-bis(n-thienyl)-1,3,4-thiadiazoles: electrochemical, X-ray photoelectron spectroscopy and theoretical studies. Appl Surf Sci 253:9267–9276
Li M, Liu X, Liu N, Guo Z, Singh PK, Fu S (2018) Effect of surface wettability on the antibacterial activity of nanocellulose-based material with quaternary ammonium groups. Colloid Surf A 554:122–128
Lin H, Yao L R, Chen Y Y, Wang H (2008) Structure and properties of silk fibroin modified cotton. Fibers Polym 9(2):113–120
Liu W, Wu Y, Wang C, Li HC, Wang T, Liao CY, Cui L, Zhou QF, Yan B, Jiang GB (2010) Impact of silver nanoparticles on human cells: effect of particle size. Nanotoxicology 4:319–330
Liu ZH, Fatehi P, Sadeghi S, Ni YH (2011) Application of hemicelluloses precipitated via ethanol treatment of pre-hydrolysis liquor in high-yield pulp. Bioresour Technol 102:9613–9618
Luo H, Lan H, Cha R, Yu X, Gao P, Zhang P, Han L, Jiang, X (2021) Dialdehyde Nanocrystalline Cellulose as Antibiotic Substitutes against Multidrug-Resistant Bacteria. ACS Appl Mater Interfaces 13(29):33802–33811
Mascotti ML, Bisogno F, Lima B, Kurina-Sanz M, Feresin GE, Enriz RD, Giannini FA (2010) Antibacterial activity of phenylpropanoids derived from cinnamic acid. Lat Am J Pharm 29:1035–1037
Maunu S, Liitiä T, Kauliomäki S, Hortling B, Sundquist J (2000) ^{13}C CPMAS NMR investigations of cellulose polymorphs in different pulps. Cellulose 7:147–159
Mayer S, Tallawi M, Luca ID, Calarco A, Reinhardt N, Gray LA, Drechsler K, Moeini A, Germann N (2021) Antimicrobial and physicochemical characterization of 2,3-dialdehyde cellulose-based wound dressings systems. Carbohydr Polym 272:118506
Mou K, Li J, Wang Y, Cha R, Jiang X (2017) 2,3-Dialdehyde nanofibrillated cellulose as a potential material for the treatment of MRSA infection. J Mater Chem B 5(38):7876–7884
Natella F, Nardini M, Di Felice M, Scaccini C (1999) Benzoic and cinnamic acid derivatives as antioxidants: structure-activity relation. J Agric Food Chem 47:1453–1459
Park D, Wang J, Klibanov AM (2006) One-step painting-like coating procedures to make surfaces highly and permanently bactericidal. Biotechnol Prog 22:584–589
Park S, Baker JO, Himmel ME, Parilla PA, Johnson DK (2010) Research cellulose crystallinity index: measurement techniques and their impact on interpreting cellulase performance. Biotechnol Biofuels 3:10
Poças MF, Oliveira JC, Pereira JR, Hogg T (2010) Consumer exposure to phthalates from paper packaging: an integrated approach. Food Addit Contam 27:1451–1459
Rostami M, Yousefi M, Khezerlou A, Mohammadi MA, Jafari SM (2019) Application of different biopolymers for nanoencapsulation of antioxidants via electrohydrodynamic processes. Food Hydrocoll 97:105170
Saini S, Belgacem MN, Salon M-CB, Bras J (2016a) Non leaching biomimetic antimicrobial surfaces via surface functionalisation of cellulose nanofibers with aminosilane. Cellulose 23:795–810
Saini S, Falco CY, Belgacem MN, Bras J (2016b) Surface cationized cellulose nanofibrils for the production of contact active antimicrobial surfaces. Carbohydr Polym 135:239–247
Saini S, Belgacem MN, Bras J (2017) Effect of variable aminoalkyl chains on chemical grafting of cellulose nanofiber and their antimicrobial activity. Mater Sci Eng C 75:760–768
Siller M, Amer H, Bache M, Roggenstein W, Rosenau T, Potthast A (2015) Effects of periodate oxidation on cellulose polymorphs. Cellulose 22:2245–2261
Song X, Zhang L, Wang Y, Zhao R, Sun X, Tian Y, Sun R, Hua C, Bai R, Wang C, Gao S (2022) Long term antibacterial effect cellulose film was modified with polyhexamethylene biguanide (PHMB). Ind Crop Prod 184:115038

Sova M (2012) Antioxidant and antimicrobial activities of cinnamic acid derivatives. Mini-Rev Med Chem 12:749–767
Sun B, Hou QX, Liu ZH, Ni YH (2015a) Sodium periodate oxidation of cellulose nanocrystal and its application as a paper wet strength additive. Cellulose 22:1135–1146
Sun X, Wu Q, Ren S, Lei T (2015b) Comparison of highly transparent all-cellulose nanopaper prepared using sulfuric acid and TEMPO-mediated oxidation methods. Cellulose 22:1123–1133
Sun L, Yang S, Qian X, An X (2020) High-efficacy and long term antibacterial cellulose material: anchored guanidine polymer via double "click chemistry." Cellulose 27:8799–8812
Tavakolian M, Jafari SM, van de Ven TG (2020) A review on surface-functionalized cellulosic nanostructures as biocompatible antibacterial materials. Nanomicro Lett 12(1):1–23
Tiller JC, Liao C-J, Lewis K, Klibanov AM (2001) Designing surfaces that kill bacteria on contact. Proc Natl Acad Sci USA 98:5981–5985
Visakh PM, Thomas S (2010) Preparation of bionanomaterials and their polymer nanocomposites from waste and biomass. Waste Biomass Valoriz 1:121–134
Wang R, Xue H, Leng J, Zhang J, Yan Z, Liu X, Feng H, Xiao L, Zhu W (2022) Preparation and antibacterial properties of hemp cellulose-based material based on Schiff base between lysine grafted N-halamine and dialdehyde hemp. Ind Crop Prod 176:114388
Wei L, Song J, Cheng B, Yang Z (2020) Synthesis, characterization and antibacterial properties of novel cellulose acetate sorbate. Carbohydr Polym 243:116416
Weishaupt R, Zünd JN, Heuberger L, Zuber F, Faccio G, Robotti F, Ferrari A, Fortunato G, Ren Q, Maniura-Weber K, Géraldine Guex A (2020) Antibacterial, cytocompatible, sustainably sourced: cellulose membranes with bifunctional peptides for advanced wound dressings. Adv Healthc Mater 9:e1901850
Whitney BM, Williams RC, Eifert J, Marcy J (2008) High pressures in combination with antimicrobials to reduce Escherichia coli O157:H7 and salmonella agona in apple Juice and orange juice. J Food Prot 71:820–824
Wu Y, Li Q, Zhang X, Li Y, Li B, Liu S (2019) Cellulose-based peptidopolysaccharides as cationic antimicrobial package films. Int J Biol Macromol 128:673–680
Xu Y, Shi Y, Lei F, Dai L (2020) A novel and green cellulose-based Schiff base-Cu (II) complex and its excellent antibacterial activity. Carbohydr Polym 230:115671
Xu Y, Xu Y, Deng W, Chen H, Xiong J (2023) Extracting dialdehyde cellulose nanocrystals using choline chloride/urea-based deep eutectic solvents: a comparative study in $NaIO_4$ pre-oxidation and synchronous oxidation. Int J Biol Macromol 246:125604
Yin N, Du R, Zhao F, Han Y, Zhou Z (2019) Characterization of antibacterial bacterial cellulose composite membranes modified with chitosan or chitooligosaccharide. Carbohydr Polym 229:115520
Zhang L, Ge H, Xu M, Cao J, Dai Y (2017) Physicochemical properties, antioxidant and antibacterial activities of dialdehyde microcrystalline cellulose. Cellulose 24:2287–2298
Zhang L, Yan P, Li Y, He X, Dai Y, Tan Z (2020) Preparation and antibacterial activity of a cellulose-based Schiff base derived from dialdehyde cellulose and L-lysine. Ind Crops Prod 145:112126
Zhang Z, Whitten DG, Kell A (2022) Fluorescent cellulose wipe as a new and sustainable light-activated antibacterial and antiviral agent. ACS Mater Lett 4:356–362
Zhang Y, Deng W, Liu C, Yan F, Wu M, Cui Q, Willför S, Xu C, Li B (2023) Preparation of antibacterial dialdehyde nanocellulose using $LiBr{\cdot}3H_2O$ non-dissolving pretreatment promoted periodate oxidation. ACS Sustain Chem Eng 11:6641–6651
Zhao M, Qi Z, Chen F, Yue X (2014) Kinetics of nonIsothermal decomposition of cinnamic acid. Russ J Phys Chem A 88(7):1081–1084
Zmejkoski DZ, Markovic ZM, Mitic DD, Zdravkovic NM, Kozyrovska NO, Bugarova N, Markovic BMT (2022) Antibacterial composite hydrogels of graphene quantum dots and bacterial cellulose accelerate wound healing. J Biomed Mater Res Part B Appl Biomater 110:1796–1805

Publisher's Note Springer Nature remains neutral with regard to jurisdictional claims in published maps and institutional affiliations.